

# Structural, Optical, Luminescent and Magnetic Properties of Spray Deposited ZnS, ZnS:Mn and ZnS:Cu Thin Films

G. Selvan<sup>1,2,\*</sup> and R. Thiagarajan<sup>1</sup>

<sup>1</sup>Department of Physics, Urumu Dhanalakshmi College, Kattur, Tamilnadu, India; gselvan96@gmail.com, rtrudc1962@gmail.com

<sup>2</sup>Department of Physics, Thanthai Hans Roever College, Perambalur, Tamilnadu, India

## Abstract

**Objectives:** The study aims to investigate the structural, morphological, optical, luminescent and magnetic properties of undoped, Mn-doped, Cu-doped ZnS thin films. **Method/Statistical analysis:** Spray technique is adopted to deposit the films on glass substrates maintained at 400 °C. The deposited films were characterized by various techniques to justify the objectives. **Findings:** The undoped and doped ZnS thin films exhibit cubic crystal structure with band gap values of ZnS, ZnS:Mn and ZnS:Cu thin films being 3.83, 3.79 and 3.74 eV, respectively. Pure ZnS exhibits diamagnetic behaviour; whereas the ZnS:Mn and ZnS:Cu thin films show paramagnetic and weak ferromagnetic behaviour, respectively. **Application/improvements:** The presence of blue, green and yellow band emissions and weak ferromagnetism realized for the ZnS:Cu thin film confirms its utility in luminescent devices and spintronic device applications.

**Keywords:** Structural, Optical, Luminescence, Spray Deposition, Thin Films

## 1. Introduction

The physical properties of materials in low dimensions like a blue shift in the optical absorption spectrum, increased effective surface area, reactivity, phase-phase transformation, strength, etc makes nanomaterials receive much more attention of research in recent years. Nanostructured metal chalcogenide thin films are used in light-emitting diodes, photo-conductive devices, solar cells, lasers, optical waveguides, and sensors.

Among the metal chalcogenides, zinc sulfide (ZnS) an important II-VI group semiconductor finds applications in lasers, solar cells, photovoltaic devices, luminescent displays, etc due to its better optical properties.<sup>1</sup> ZnS exhibits zinc blende (cubic phase) and wurtzite (hexagonal phase) structures with bandgap energies of 3.54 eV and 3.80 eV, respectively.<sup>2</sup> The energy band characteristics

of ZnS make it useful as a phosphor and in thin-film electroluminescent devices.<sup>3</sup> In laser, nonlinear optical, electroluminescent, photoluminescent, spintronic and quantum devices, dilute magnetic semiconductors (DMSs) are widely used.<sup>4</sup> Even though ZnS possess significant optical and luminescent properties, its use as DMS is very much restricted due to its paramagnetic behaviour. To utilize ZnS for spintronic applications, its magnetic behaviour must be enhanced which can be achieved through doping. Ferromagnetic orderings in ZnS has been realized with Co doping by.<sup>5</sup> Ferromagnetic stable state and half metallicity have been realized in ZnS through Fe doping by.<sup>6</sup> Cr-doped ZnS showed partially filled intermediate band for both FM and AFM spin alignments.<sup>7</sup> Strong p-d hybridization between sulfur and transition metal ions are supposed to induce ferromagnetic stable state in ZnS.<sup>8</sup> In the present work, manganese (Mn)

\*Author for correspondence

and copper (Cu) has been used as dopant ions to induce ferromagnetic orderings in spray deposited ZnS thin films. In addition to the magnetic properties, optical and luminescent properties were studied and reported.

## 2. Experimental Details

Spray pyrolysis technique is used to deposit undoped, Mn-doped and Cu-doped ZnS thin films. Zinc acetate [ $\text{Zn}(\text{CH}_3\text{COO})_2 \cdot 2\text{H}_2\text{O}$ ] and thiourea [ $\text{SC}(\text{NH}_2)_2$ ] are used as the precursor salts to prepare ZnS thin films. 0.1 M of zinc acetate and 0.2 M of thiourea were dissolved in 50 mL de-ionized water and sprayed on glass substrates heated at 400 °C. Due to pyrolytic decomposition, ZnS thin films were deposited. To accomplish Mn and Cu doping, manganese acetate and cupric chloride each of 5 wt.% of zinc acetate was added to the precursor solution and sprayed. XRD spectra, SEM images, optical band gap were obtained using X'Pert PRO Analytical PW 340/60 X-ray diffract meter, HITACHI S-3000H scanning electron microscope and LAMBDA-35 UV-vis-NIR double beam spectrophotometer, respectively.

PL spectra and M-H curves were drawn using Varian Cary Eclipse fluorescence spectrometer and Lakeshore 7410 vibrating sample magnetometer, respectively.

## 3. Results and Discussion

### 3.1 Structural Studies

Figure 1 pictures the XRD patterns of undoped, Mn and Cu-doped ZnS thin films. All the films exhibit a cubic crystal structure of ZnS (JCPDS Card No. 05-0566). A strong (1 1 1) preferential growth is realized for all the films. No shift in the (1 1 1) peak position is observed for the ZnS:Cu thin films as the ionic radius of  $\text{Cu}^{2+}$  (0.72 Å) is almost comparable to that of  $\text{Zn}^{2+}$  (0.74 Å). However, a shift towards a smaller  $2\theta$  angle observed for the ZnS:Mn thin film is due to the fact that  $\text{Mn}^{2+}$  (0.80 Å) ion possesses a larger ionic radius than  $\text{Zn}^{2+}$  ion. The lattice parameter values calculated using the relation,  $1/d^2 = \alpha^2/(h^2 + k^2 + l^2)$  were 5.396, 5.399 and 5.395 Å, respectively for the undoped ZnS, ZnS:Mn and ZnS:Cu thin films. Using the Scherrer formula,  $D = 0.9\lambda/\beta\cos\theta$ , the crystallite size of the films was calculated and found to be 39, 36 and 30 nm, respectively for the ZnS, ZnS:Cu and ZnS:Mn thin films. The decreased crystallite size value observed for the

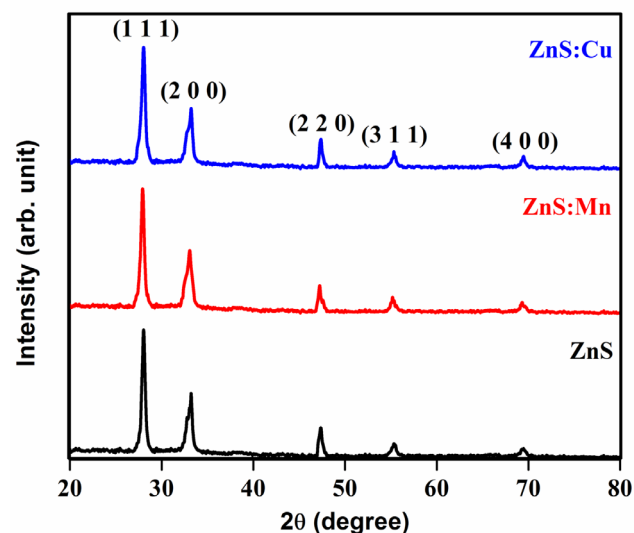


**Figure 1.** XRD patterns of ZnS, ZnS:Cu and ZnS:Mn thin films.

doped films might be due to the drag force exerted by the dopant ions on boundary motion and grain growth.

### 3.2 SEM Analysis

Figure 2 shows the SEM images of a) ZnS, b) ZnS:Mn and c) ZnS:Cu thin films. Grains appear to be clustered for pure ZnS. With Mn doping no clustering takes place and the surface got modified with spherical and cubical grains. Nanoneedles are also seen along with few flower shaped grains. The surface of ZnS got modified with uniformly shaped grains with Cu doping. Few cloudy regions are also visible.

### 3.3 Optical Studies

From the transmittance spectra (Figure 3), all the films are found to be highly transparent in the visible region with steep optical edges. Both the ZnS:Mn and ZnS:Cu thin films exhibit better transparency than the pure ZnS thin film, which might be due to narrow grains size distribution as well as low concentration of defects, such as pits and voids in the films. From the Tauc plots (Figure 4), the bandgap ( $E_g$ ) values of the ZnS, ZnS:Mn and ZnS:Cu thin films was estimated by extrapolating the straight-line portion to zero absorption coefficient value<sup>9</sup> and was found to be 3.83, 3.79 and 3.74 eV, respectively. The reduction in the bandgap values involves the formation of new energy levels close to the valence band edge which

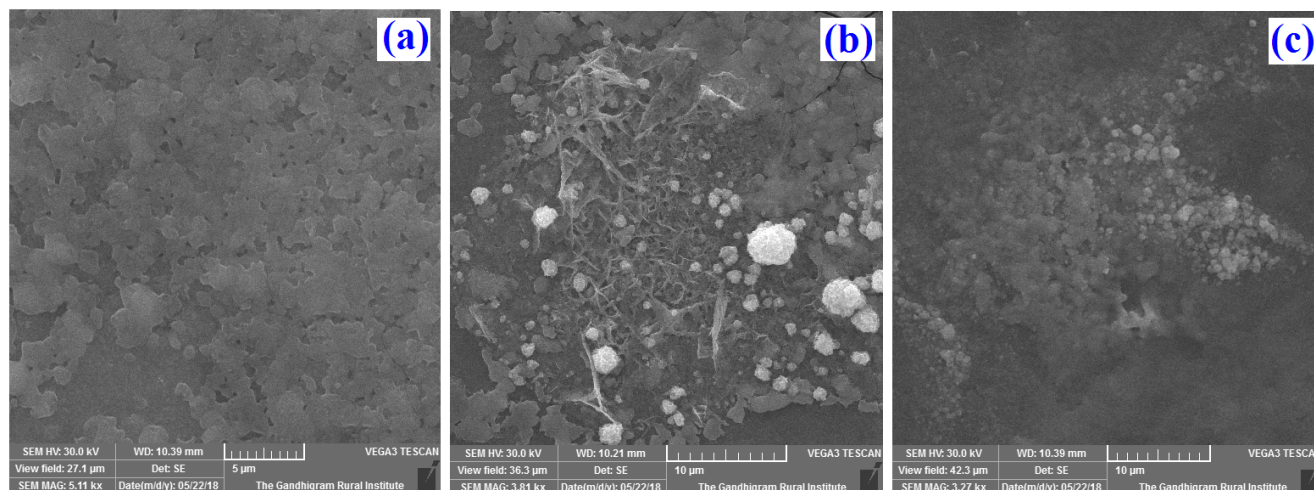


**Figure 2.** SEM images of a) ZnS, b) ZnS:Cu and c) ZnS:Mn thin films.

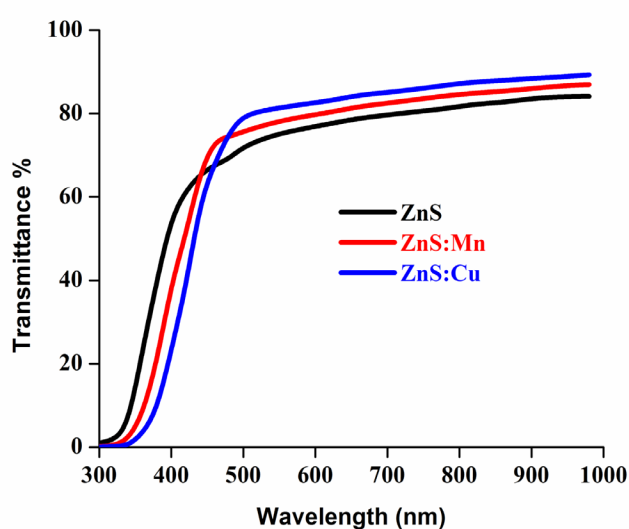


**Figure 3.** Transmittance spectra of the ZnS, ZnS:Cu and ZnS:Mn thin films.

are associated with structural defects.<sup>10</sup> The decreased bandgap values observed with doping may be attributed to the Mass-Burstein effect according to which electron-electron interaction takes place due to increased carrier concentration and hence optical shrinkage is realized.

### 3.4 PL Studies

The room temperature PL spectra of ZnS, ZnS:Cu and ZnS:Mn thin films excited at  $\lambda = 350$  nm are shown in Figure 5. The near band edge (NBE) emission peaks

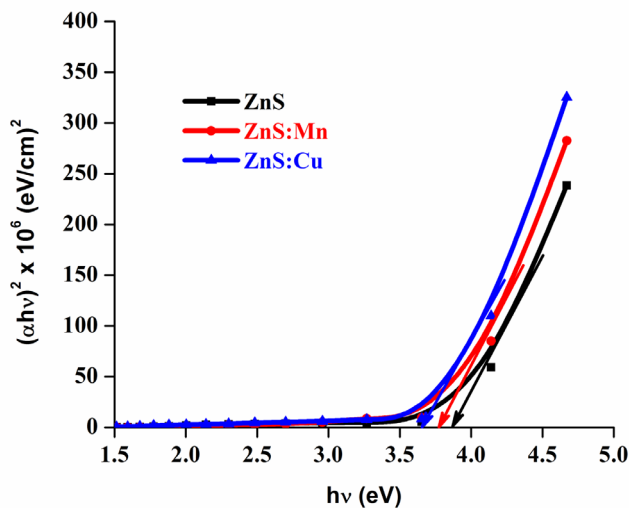


**Figure 4.** Tauc plots of the ZnS, ZnS:Cu and ZnS:Mn thin films.

observed at 361, 377 nm for pure ZnS, at 360, 372, 384, 391 nm for the ZnS:Cu and at 361, 376 nm for the ZnS:Mn thin films are attributed to free exciton annihilation.<sup>11</sup> The recombination between the sulfur-vacancy related donor and the valence band results in the emission of peaks at 411 nm for ZnS, ZnS:Cu and at 410 nm for ZnS:Mn thin films. Interstitial sulfur lattice defects are responsible for the emission peaks at 437 nm for pure ZnS and ZnS:Cu and at 436 nm for the ZnS:Mn thin films. The blue emission peaks observed at 461, 491 nm for the ZnS:Cu at 490 nm for pure ZnS, at 491 nm for the ZnS:Mn thin films are due to the transitions of trapped electrons to the valence band.

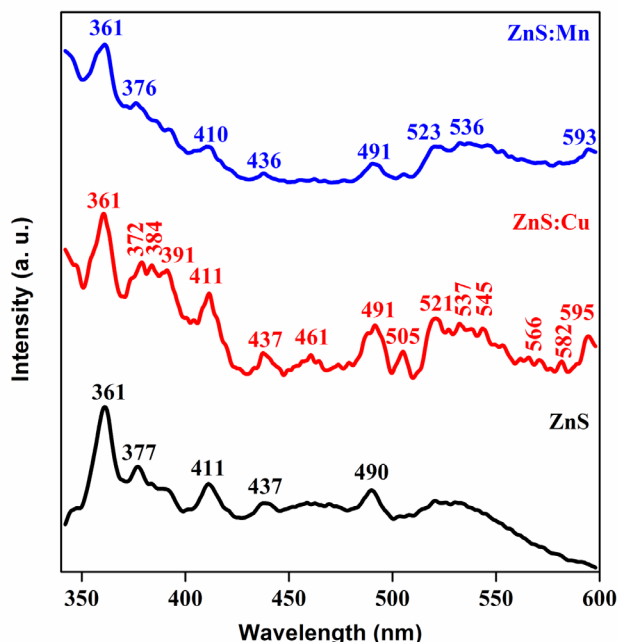


**Figure 5.** PL spectra of the ZnS, ZnS:Cu and ZnS:Mn thin films.

Electron-hole recombination at trap or imperfection sites is responsible for the emission peaks at 505, 521, 532 nm for the ZnS:Cu and at 523 nm for the ZnS:Mn thin films. The sulfur species on the surface of the films contribute to the emission of the peak at 545 nm for the ZnS:Cu thin film.<sup>12</sup> Emission peaks related to metal interstitials are observed at 566 and 582 nm for the ZnS:Cu thin film.<sup>13</sup> Donor acceptor pair (DAP) related peaks are observed at 595 nm for the ZnS:Cu and at 593 nm for the ZnS:Mn thin films.<sup>14</sup> The presence of blue, green and yellow band emissions observed for the ZnS:Cu thin films confirm its utility in optical luminescent devices.

### 3.5 Magnetic Studies

The room temperature M-H curves of pure ZnS, ZnS:Mn and ZnS:Cu thin films are displayed in Figure 6. Undoped ZnS exhibits diamagnetic behaviour; whereas the ZnS:Mn thin film show paramagnetic behaviour and the ZnS:Cu thin film exhibits ferromagnetic behaviour. Similar

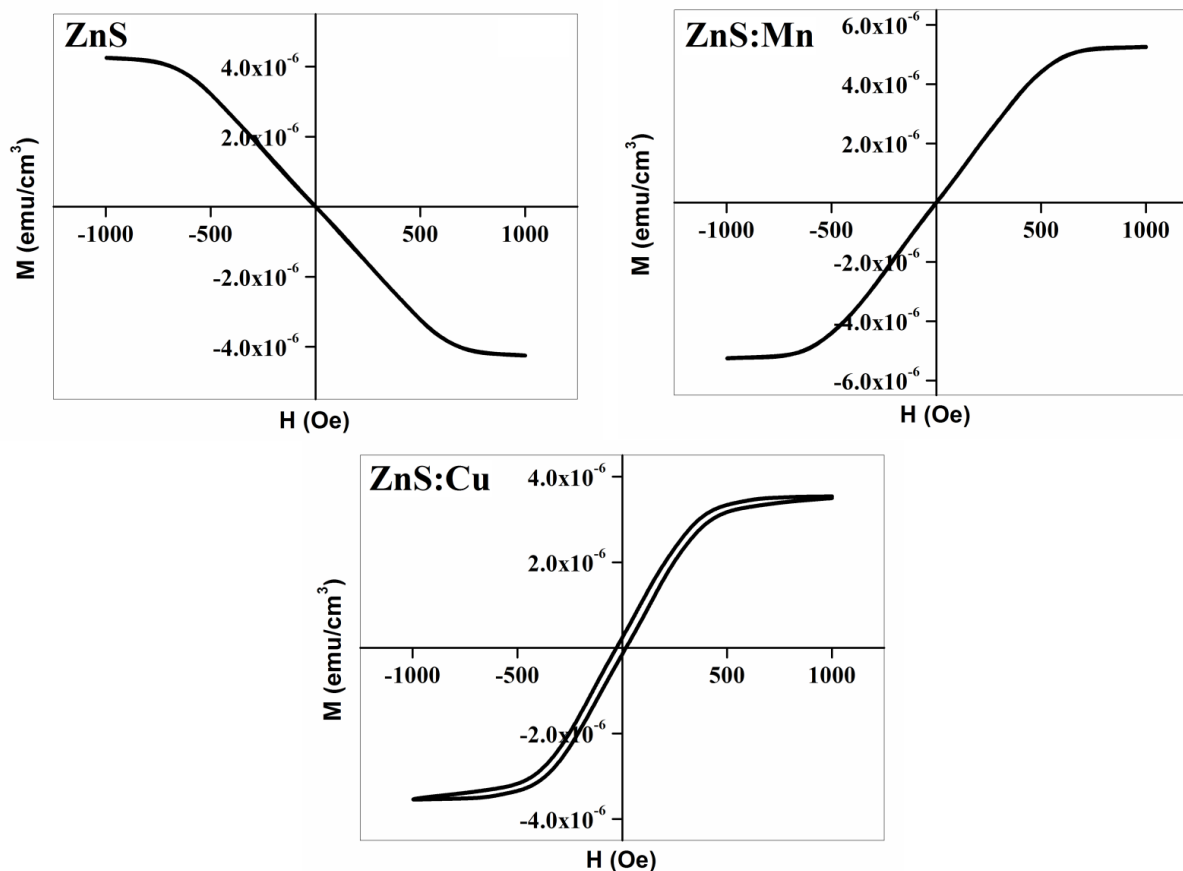


**Figure 6.** M-H curves of the ZnS, ZnS:Cu and ZnS:Mn thin films.

diamagnetic behaviour has been reported earlier for pure ZnS thin film by.<sup>6</sup> When ZnS is doped with Mn, localized spins are provided.

If free carriers are present in the ZnS matrix, then there might be exchange interaction between the local spin-polarized electrons (electrons of  $Mn^{2+}$  ions) and the free electrons, which leads to their spin polarization effect. Subsequently, the spin-polarized free electrons perform an exchange interaction with local spin-polarized electrons of other  $Mn^{2+}$  ions. Thus, after the long-exchange interaction, almost all  $Mn^{2+}$  ions exhibit the same spin direction, as a result, paramagnetic nature is realized for the ZnS:Mn thin film.<sup>15</sup> In the case of ZnS:Cu thin film, ferromagnetism is due to the magnetic interactions between the doped  $Cu^{2+}$  ions or from the substitution spin-polarized Cu atoms in the ZnS lattice.<sup>16</sup> Vacancy driven  $d^0$  FM mechanism also contributes to the ferromagnetic behaviour of the ZnS:Cu thin film.<sup>17</sup>

## 4. Conclusion

Thin films of ZnS, Cu-doped ZnS, and Mn-doped ZnS were deposited using the spray pyrolysis technique on glass substrates. From the studies performed it was observed that Cu and Mn doping has a profound influence on the properties of pure ZnS. Improved magnetic properties observed for the ZnS:Mn and ZnS:Cu thin films confirmed their potential for spintronic device applications.

## References

1. Firdous A, Aslam Baba M, Singh D, Bhat AH. Optical and impedance studies of pure and Ba-doped ZnS quantum dots. *Appl Nanosci.* 2015;5(2):201–6.
2. Hitkari G, Singh S, Pandey G. Structural, optical and photocatalytic study of ZnO and ZnO-ZnS synthesized by chemical method. *Nano Struct Nano Objects.* 2017:1–9.
3. Yang Y, Huang J, Yang B, Liu S, Shen J. Electroluminescence from ZnS/CdS nanocrystals/polymer composite. *Synth Metals.* 1997;91(1-3):347–49.
4. Goktas A, Mutlu IH. Structural, optical and magnetic properties of solutions-processed Co-doped ZnS thin films. *J Electron Mater.* 2016;45(11):5709–20.
5. Patel SP, Pivin JC, Chawla AK, Chandra R, Kanjilal D, Kumar L. Room temperature ferromagnetism in  $Zn_{1-x}Co_xS$  thin films with wurtzite structure. *J Magn Magn Mater.* 2011;323(22):2734–40.
6. Akhtar MS, Riaz S, Hussain SS, Naseem S. Magnetic properties of undoped and Fe-doped ZnS thin films. *Adv Civ Environ Mater Res.* 2014, 1, pp. 24–28.
7. Tablero C. Electronic and magnetic properties of ZnS doped with Cr. *Phys Rev B.* 2006;74(19):195203–11.
8. Chen HX, Shi DN, Qi JS, Wang BL. First principles study on the magnetic properties of transition metal atoms doped  $(ZnS)_{12}$  clusters. *J Magn Magn Mater.* 2011;323(6):781–88.
9. Narasimman V, Nagarethinam VS, Selvan G, Abubacker MP, Balu AR. Bromine doping effect on some properties of CdS films. *Surf Eng.* 2017;33(3):175–80.
10. Coronado EGA, Gonzalez LA, Angeles JCR, Melendez-Lira MA, Ramirez-Bon R. Study of the structure and optical properties of Cu and Mn in situ doped ZnS films by chemical bath deposition. *Mater Sci Semicond Process.* 2018;81:68–74.
11. Ravishankar S, Balu AR, Balamurugan S, Usharani K, Prabha D, Suganya M, et al. TG-DTA analysis, structural, optical and magnetic properties of PbS thin films doped with  $Co^{2+}$  ions. *J Mater Sci Mater Electron.* 2018;29(7):6051–58.
12. Suganya M, Balu AR, Anitha S, Prabha D, Balamurugan S, Priyanka B, et al. PbS-NiO nanocomposite material with enhanced magnetic, photocatalytic and antifungal properties. *Mater Sci Eng B.* 2018;229:118–25.
13. Narasimman V, Nagarethinam VS, Usharani K, Balu AR. Optoelectronic, magnetic and antibacterial properties of Zr-doped CdS thin films. *Optik.* 2017;138:398–406.
14. Abubacker MP, Selvan G, Balu AR. Optoelectronic, magnetic and antifungal properties of CdS thin films co-doped with zinc and bromine. *J Mater Sci Mater Electron.* 2017;28(14):10433–40.
15. Wang J, Wan J, Chen K. Facile synthesis of superparamagnetic Fe-doped ZnO nanoparticles in liquid polyols. *Mater Lett.* 2010;64(21):2373–75.
16. Yildirim OA, Durucan C. Room temperature synthesis of Cu incorporated ZnO nanoparticles with room temperature ferromagnetic activity: structural, optical and magnetic characterization. *Ceram Int.* 2016;42(2):3229–38.
17. Srivind J, Nagarethinam VS, Suganya M, Balamurugan S, Usharani K, Balu AR. NiO coupled  $SnS_2$  nanoparticles with improved magnetic and photocatalytic performance against the degradation of organic dyes without N=N double bond. *Vacuum.* 2019;163(1):373–83.